Microfabrication of poly(acrylamide) hydrogels with independently controlled topography and stiffness

Jordi Comelles[1,*], Vanesa Fernández-Majada[1], Núria Berlanga-Navarro[1], Verónica Acevedo[1], Karolina Paszkowska[1] and Elena Martínez[1,2,3,*]

[1]Institute for Bioengineering of Catalonia (IBEC), The Barcelona Institute of Science and Technology (BIST), c/ Baldiri Reixac 10-12, 08028, Barcelona, Spain
[2]Centro de Investigación Biomédica en Red (CIBER), Av. Monforte de Lemos 3-5, Pabellón 11, Planta 0, 28029 Madrid, Spain
[3]Department of Electronics and Biomedical Engineering, University of Barcelona (UB), c/Martí i Franquès 1-11, 08028 Barcelona, Spain

E-mail: emartinez@ibecbarcelona.eu, jcomelles@ibecbarcelona.eu

Received xxxxxx
Accepted for publication xxxxxx
Published xxxxxx

Abstract

The stiffness and topography of a cell's extracellular matrix are physical cues that play a key role in regulating processes that determine cellular fate and function. While substrate stiffness can dictate cell differentiation lineage, migration, and self-organization, topographical features can change the cell's differentiation profile or migration ability. Although both physical cues are present and intrinsic to the native tissues *in vivo*, *in vitro* studies have been hampered by the lack of technological set-ups that would be compatible with cell culture and characterization. *In vitro* studies therefore either focused on screening stiffness effects in cells cultured on flat substrates or on determining topography effects in cells cultured onto hard materials. Here, we present a reliable, microfabrication method to obtain well defined topographical structures of micrometer size (5-10 µm) on soft polyacrylamide hydrogels with tunable mechanical stiffness (3-145 kPa) that closely mimic the *in vivo* situation. Topographically microstructured polyacrylamide hydrogels are polymerized by capillary force lithography using flexible materials as molds. The topographical microstructures are resistant to swelling, can be conformally functionalized by extracellular matrix proteins and sustain the growth of cell lines (fibroblasts and myoblasts) and primary cells (mouse intestinal epithelial cells). Our method can independently control stiffness and topography, which allows to individually assess the contribution of each physical cue to cell response or to explore potential synergistic effects. We anticipate that our fabrication method will be of great utility in tissue engineering and biophysics, especially for applications where the use of complex *in vivo*-like environments is of paramount importance.

Keywords: microstructured hydrogels; topography; substrate stiffness; polyacrylamide; contact guidance; myotube differentiation; intestinal epithelial cells

1. Introduction

Hydrogels have become increasingly popular as matrices in *in vitro* cell culture since both natural [1] and synthetic [2] polymers offer the cells properties similar to those of their native extracellular matrix (ECM). Such *in vivo*-like microenvironments trigger cell behaviors that may substantially differ from those observed on conventional rigid substrates. For example, breast epithelial cells self-organize in 3-dimensional (3D) structures when cultured on hydrogels [3], mouse embryonic stem cells maintain pluripotency when grown on soft hydrogels that match stem cell intrinsic stiffness [4], and resistance to chemotherapy can be modulated when a tumor grows on artificial hydrogels [5].

Polyacrylamide (PA) hydrogels significantly advanced our understanding of the role played by mechanical properties in triggering a cell response. One of the main reasons for this success is that PA hydrogel stiffness can be easily tuned by simply changing the ratio of acrylamide to bis-acrylamide components in the co-polymer. In addition, PA hydrogels can be functionalized in a simple and effective manner using proteins to better mimic the native ECM composition and render them bioactive. For instance, PA hydrogels have been used to show that stem cells can commit to specific phenotypes with exquisite sensitivity to the underlying substrate stiffness [6]. Moreover, using PA hydrogels it has been proved that both single [7] and collective [8] cell migration can be directed by stiffness gradients in a process known as *durotaxis*. Finally, PA hydrogels combined with sub-micrometer sized fluorescence beads are the gold-standard for substrates used in traction force microscopy (TFM) [9,10] to describe the mechanical signature of single [9,11] and collective [10] cell migration and division [12].

Despite the significant advancements afforded by the use of PA hydrogels, most studies employed PA hydrogel thin films bound to coverslips that expose cells to flat and featureless surfaces. Conversely, it has been demonstrated *in vivo* that tissue-specific complex ECM geometries are highly relevant physical cues for physiological and pathological processes [13]. For example, stem cells in the corneal limbus are known to be confined to micrometer-sized topographical ridges, the so-called palisades of Vogt [14]. Such topographically confined stem cell niches have also been identified in other epithelial tissues such as the intestine [15] or the skin [16] and are pivotal for tissue homeostasis. Furthermore, the organization of collagen bundles in parallel topographical tracks has been associated to local cancer invasion *in vivo* [17] and identified as a negative prognostic factor for different cancers [18]. When included in *in vitro* experiments, topographical features can enhance cell differentiation of linages such as osteoblast [19], muscle [20], and chondrocyte [21]. In addition, they are able to direct axon growth [22] and cell migration through different processes such as contact guidance [23–25], *topotaxis* [26], or *ratchetaxis* [27–29]. However, the vast majority of these topography sensing studies are performed on very stiff materials such as silicon, titanium, quartz, thermoplastic polymers, or polydimethylsiloxane (PDMS) [24,30–35]. These possess elastic moduli of the order of several MPa and are thus much greater than the tissue stiffness values found *in vivo*, which are typically in the range of 1-100 kPa [36]. The incorporation of controlled microtopography on soft hydrogels could therefore be instrumental to better mimic the in vivo physical cues present in the cell's microenvironment. It would allow the study of cellular processes such as migration or differentiation into physiologically more relevant environments with regard to both architecture and stiffness.

Several studies have addressed the fabrication of microtopographical patterns on hydrogels. For instance, cell-size scale features (<10 µm) have been obtained on poly(ethylene glycol) diacrylate (PEGDA) hydrogels by using UV-photocrosslinking in PDMS molds. Soft PEGDA hydrogels (elastic moduli ~ 100 kPa) can be produced by adequately selecting the molecular weight of the polymer. However, in practice, the large swelling capability of PEG-based materials heavily distorts the topographical patterns. This prevents a faithful microtopography from developing if the elastic modulus is below 250 kPa [37] (*in vivo* tissues typically have a much lower elastic modulus). On the other hand, a few reports employed replica molding techniques to obtain topographical patterns on soft PA hydrogels [38–40]. These studies proved the relevance of both physical cues (architecture and stiffness) to study *in vitro* cell differentiation and epithelial-to-mesenchymal transition processes in confined microenvironments. However, they all employed hard silicon molds to microstructure the PA hydrogels [38,41] and since silicon-based materials are fragile and non-compliant, this choice of material makes the demolding step extremely challenging when working with small structures (< 10 µm) and soft and sticky hydrogels (elastic moduli ~10 kPa). Silicon molds are produced by employing expensive microfabrication techniques that require dedicated instruments in a cleanroom environment. Because they are easy-to-break, conventional soft lithography PDMS counterparts are usually made from the valuable original molds and used for the routine production of topographically patterned samples. However, because of its high oxygen permeability, PA polymerization is impaired when using PDMS elastomeric molds [42,43], which may explain the lack of experimental set-ups that would allow for an easy production of substrates incorporating small microstructures on soft PA hydrogels on a routine basis.

In this report, we present a reliable method to obtain topographical structures of biologically significant sizes (5-10 µm) on PA hydrogels of a tunable and biologically relevant stiffness (3-145 kPa). Our method employs PDMS molds

attached to poly(ethylene naphthalate) (PEN) substrates to transfer the mold features to soft PA hydrogels via capillary force lithography (CFL). PEN, while being thin enough to be flexible, is a polyester derivative and constitutes a superior oxygen barrier. The set-up consists of a hybrid PEN-PDMS mold, spacers, and a glass coverslip to obtain topographical patterns on the PA hydrogels. By varying the ratio of PA components, and thus the mechanical properties of the resulting hydrogels, we could systematically characterize the ability of the hydrogels in replicating a variety of microtopographies that successfully preserved their morphologies after swelling. We demonstrate that upon conformational functionalization with extracellular matrix proteins the topographically patterned PA hydrogels: (i) sustain the growth of both cell lines (fibroblasts and myoblasts) and primary cells (mouse intestinal epithelial cells), (ii) impact cell behavior over short (adhesion and spreading) and long (differentiation) time scales, and (iii) allow primary cultures to keep both proliferative and differentiated cell populations active while impacting on their ability to spread and migrate. Overall, our set-up utilizes the advantages attributed to PA hydrogels, namely tunable stiffness and protein functionalization and the complexity of microstructured materials, while allowing for an independent control of both physical cues. We believe that these characteristics endorse our fabrication method as a valuable tool in the field of biophysics research.

2. Materials and Methods

2.1 Fabrication of microstructured PA hydrogels with tunable stiffness.

Polyacrylamide (PA) microstructured hydrogels were prepared following the experimental set-up depicted in Figure 1. First, for the preparation of the thin PDMS molds, PDMS prepolymer (Sylgard 184 Silicon Elastomer, Dow Corning) prepared at a ratio of 10:1 w/w was spun-coated onto silicon molds containing square posts, holes, or lines of 5 and 10 µm in width and 1 µm in height, forming thin membranes of 50 µm in thickness. Silicon molds were fabricated on silicon wafers by standard microfabrication processes involving UV-photolithography and reactive ion etching. PDMS was then cured overnight at 65ºC. After curing, PDMS membranes were cut into pieces including both microstructured and flat regions, which would serve as controls. Then, they were bound to 125 µm thick PEN sheets (Goodfellow) to form flexible hybrid PEN-PDMS molds. In parallel, pools were created by employing purposely cut PDMS membranes (100 to 150 µm in thickness) as spacers and binding them to silanized glass coverslips (24 mm x 24 mm). Glass silanization ensured the stable attachment of PA hydrogels as described previously [44]. Briefly, "squeaky clean" [45] coverslips were stored in ethanol and dried with N_2 before use. Dried coverslips were incubated for 10 minutes with a 50% (v/v) solution of 3-(aminopropyl)trimethoxysilane (Sigma-Aldrich) in Milli-Q water, followed by an incubation with Milli-Q water for 30 minutes on an orbital shaker. Next, coverslips were rinsed multiple times with H_2O and incubated with a 0.5% (v/v) solution of glutaraldehyde (Sigma-Aldrich) in water for another 30 minutes on an orbital shaker. Finally, coverslips were rinsed several times with H_2O, dried with N_2, and stored in a vacuum desiccator until use.

PA hydrogels were prepared by copolymerizing acrylamide and bis-acrylamide (BioRad) as described previously [44,46]. Hydrogels of different stiffnesses were generated by mixing different concentrations of the two components (see Table 1) in a solution containing 0.05% (w/v) ammonium persulfate (Serva) and 1% (v/v) tetramethylethylenediamine (TEMED) (Sigma-Aldrich). To produce PA microstructured hydrogels, 80 µl of the prepolymer solutions were poured into the dedicated pools (Figure 1) containing the silanized glass coverslips. Immediately after, the hybrid PEN-PDMS mold was placed on top to let the microstructures be filled in by capillary force. PA hydrogels were then kept at room temperature for 2 h to polymerize. The polymerized hydrogels were demolded by carefully removing the flexible mold and then stored in PBS at 4ºC until further use, allowing them to achieve equilibrium swelling.

2.2 Swelling studies on the topographical features.

We systematically studied the morphological changes induced in the patterned microstructures due to the swelling of the PA hydrogels as a function of hydrogel stiffness and microstructure geometry and size. The stiffness of the samples used is indicated in Table 1. Images of the microstructured hydrogels were obtained by phase contrast microscopy (Nikon Eclipse Ts2) immediately after microfabrication as well as 24 h and 48 h after having been kept in PBS at 4ºC. Images were analyzed with Image J software (http://rsb.info.nih.gov/ij, NIH). In every image, the area and perimeter of the holes or posts were assessed and relative changes in area over time, t, due to swelling were computed as A(t)/A(mold), where A(mold) is the area of the features in the original PDMS mold. Moreover, the deformation of the microstructures due to swelling was quantitatively assessed by defining a squareness parameter, S, which relates the feature area to its corresponding perimeter, P, through:

$$S(t) = \frac{(A(t))}{\left(\frac{P(t))}{4}\right)^2} \qquad (1)$$

By definition, S = 1 for a perfect square (see Figure 4C).

2.3 Atomic force microscopy (AFM) to measure stiffness and obtain topographical images of the PA microstructured hydrogels.

Young's moduli of the microstructured PA hydrogels were measured in liquid conditions after 48 h of swelling (see section 2.2) with and without protein functionalization on microstructured regions following a previously described protocol [47]. In short, we used a NanoWizard® 4 Bioscience AFM (JPK Instruments) mounted onto a Nikon Ti inverted microscope to perform indentation measurements. Silicon nitride pyramidal tips (NanoWorld) with nominal spring constants of 0.32 $N \cdot m^{-1}$ or 0.08 $N \cdot m^{-1}$ were used. Three different positions in the central region of each hydrogel were measured (10 indentations of 1 µm at a frequency of 0.5 Hz) for N = 3 hydrogels. To obtain the elastic modulus, the Hertz model for a pyramidal tip was fitted to the measured force-distance curves, using the proprietary JPK data analysis software. The NanoWizard® 4 AFM was also used to obtain the topographical AFM images of the microstructures. After defining a square-shaped scanning region of 20 μm^2, we obtained a force-distance curve at each pixel (256 x 256). To obtain the three-dimensional shape of the features, the cantilever was traveling a z-length of 5 µm with a dwelling time of 150 ms at each pixel. Images were reconstructed using JPK data analysis software.

2.4 Protein functionalization of the PA hydrogels.

Fibronectin from bovine serum (Sigma-Aldrich) and collagen type I (Sigma-Aldrich) were covalently bound to PA hydrogels using Sulfo-SANPAH reagent (Sigma-Aldrich). PA hydrogels were removed from their PBS storage and any excess PBS eliminated with a drying paper (via capillarity) taking care to avoid any contact with the microstructured regions. Then, we freshly prepared a Sulfo-SANPAH solution at a concentration of 2 µg/µl in Milli-Q water and added 50 µl on top of each PA hydrogel. The PA hydrogels with the Sulfo-SANPAH solution were UV-irradiated (Light Source LQ-HXP 120 UV, LEJ) for 30 seconds and then rinsed several times with PBS before drying them with drying paper to remove any excess buffer. Next, we incubated the proteins on the activated hydrogels using either 20 µl of a 20 µg/ml fibronectin solution, 200 µg/ml fibronectin solution or 100 µg/ml collagen type I solution. In order to avoid evaporation of the protein solutions, PA hydrogels were carefully covered with parafilm. Proteins were incubated for 1 h at room temperature (RT). Functionalized PA hydrogels were stored in culture medium until cell seeding.

2.5 Cell culture.

NIH 3T3 mouse embryonic fibroblasts (ATCC® CRL-1658™) and C2C12 mouse myoblasts (ATCC® CRL-1772™) were grown with DMEM (Invitrogen) medium supplemented with 10% Fetal Bovine Serum (FBS) (Life Technologies), 1% L-glutamine (Gibco), 1% penicillin-streptomycin (Sigma-Aldrich), 1% sodium pyruvate (Invitrogen) at 37ºC, and 5% CO_2. For the experiments, cells were trypsinized and seeded as individual cells onto the PA hydrogels of different stiffnesses, patterned into 5 µm wide lines or posts and functionalized with fibronectin. We chose to use line patterns for these experiments because this allows for easier read-outs of the quantitative parameters of the cell phenotype in response to topography (cell alignment and elongation). For the experiments employing NIH 3T3, 50000 cells per well (35 mm petri dish) were cultured on the PA hydrogels during 24 h. For experiments employing C2C12 mouse myoblasts, 150,000 cells per well (35 mm petri dish) were cultured during 3 days with normal culture medium (DMEM,10% Fetal Bovine Serum, 1% L-glutamine, 1% penicillin-streptomycin, and 1% sodium pyruvate) and for an additional 7 days with differentiation medium (DMEM, 10% Horse Serum (Life Technologies), 1% L-glutamine, 1% penicillin-streptomycin, and 1% sodium pyruvate). After these culturing periods, cells were imaged either by phase contrast microscopy (Nikon Eclipse Ts2) or fixed for immunostaining analysis. For NIH 3T3 cells, the effects of both stiffness and topography were established by measuring morphological parameters using Image J software (http://rsb.info.nih.gov/ij, NIH). Cell area was measured by outlining the cell shape. Cell elongation and alignment were measured from by fitting an ellipse to the cell shape. The elongation was assessed by calculating (major axis – minor axis)/ (major axis + minor axis) and the alignment index was calculated as $\cos(2\theta)$, where θ is the angle between the ellipse's major axis and the direction of the topographical pattern. For the C2C12 myoblasts, the qualitative alignment of the cells with the topography and the presence of myosin heavy chains were used as read-outs for cell morphology and cell differentiation to myotube, respectively.

Intestinal epithelial cells (IECs) were obtained through mechanical and enzymatical digestion of intestinal organoids isolated from Lgr5-EGFP-IRES-creERT2 mice [48]. IECs were cultured with advanced DMEM/F12 (Invitrogen) medium supplemented with 1% GlutaMAX (Gibco), 1% HEPES (Sigma), Normocin (Invitrogen), 2% B27 (Gibco), 1% N2 (Gibco), 1.25 mM N-acetylcysteine (Sigma) plus murine EGF (100 ng/ml, Gibco), recombinant human R-spondin 1 (200 ng/ml, R&D Biosystems), recombinant murine Noggin (100 ng/ml, Peprotech), CHIR99021 (3 µM), and valproic acid (1 mM). For the experiments, 50,000 cells were seeded as individual cells onto the PA hydrogels of different stiffnesses, patterned into lines of 5 µm in width and functionalized with collagen. After culturing for 24 h, live-cell imagery was performed using phase contrast microscopy (Axio Observer 7, Carl Zeiss) for 6 h to monitor epithelial spreading and cell trajectories. Afterwards, cells were kept in culture for 2 more days and then fixed for immunostaining analysis. In this case, cell spreading, cell trajectories, as well as differentiation and proliferation markers were used to evaluate the effects of the substrate on this cell culture type.

2.6 Cell Viability.

Cell viability on PA hydrogels was assessed using a calcein-AM/ethidium homodimer Live/Dead kit (Invitrogen) 24 hours after seeding. The test was performed with NIH 3T3 fibroblasts both on 12% Acrylamide / 0.6% Bis-acrylamide hydrogels functionalized with 20 µg/ml fibronectin and on glass bottom mattek petri dishes (Mattek). Fluorescent images were acquired using a Nikon Eclipse Ts2 inverted microscope. To determine the ratio of cell viability images were analyzed with Image J software (http://rsb.info.nih.gov/ij, NIH).

2.6 Cell immunostaining.

Cells were fixed with 10% neutralized formalin (Sigma), permeabilized with 0.5% Triton X-100 (Sigma), and blocked for at least 2 h with a blocking buffer containing 1% BSA (Sigma), 3% donkey serum (Millipore), and 0.2% Triton X-100 in PBS. The primary antibodies used were: anti-fibronectin (1:300, Sigma), anti-Ki67 (1:100, abcam), anti-cytokeratin 20 (1:100, Dako), anti-myoD monoclonal antibody (MYOD) (2 µg/ml, Sigma) and anti- Myosin Heavy Chain antibody (MYH1E) (1:5, DSHB). All samples were incubated with the primary antibodies overnight at 4°C, followed by a 1 h incubation at RT with secondary antibodies Alexa Fluor® 488 donkey anti-goat, Alexa Fluor® 488 goat anti-mouse, and Alexa Fluor® 647 donkey anti-rabbit (Jackson ImmunoResearch) diluted at 1:500. Alexa Fluor® 568 phalloidin was used to stain filamentous actin (F-actin). Nuclei were stained with 4',6-diamidino-2-phenylindole (DAPI) (1:1000). Finally, samples were mounted with Fluoromount® and observed using an Axio Observer 7 (Carl Zeiss).

2.7 Statistical analysis.

Statistical analysis was done using GraphPad Prism. Results are presented as mean ± SD or as mean ± SEM of at least N = 3 experiments. Normality of the datasets was tested by the d'Agostino-Pearson normality test. Statistical differences were analyzed by t-test or ANOVA test (Gaussian distribution) and Mann-Whitney test (non Gaussian distribution).

3. Results

3.1 Fabrication of PA hydrogels with topographical microstructures and controlled stiffness.

After 2 hours of polymer crosslinking, negative replicas of the mold on PA hydrogels were retrieved. The demolding process is made easy by the flexibility of the molds. The hydrogels were then immersed in PBS and observed under the microscope. Using our method, we were able to successfully replicate different types of structures (lines, posts and holes) on the PA hydrogels, creating topographical features of two different widths (5 µm and 10 µm) and a vertical relief height of 1 µm (Fig. 2). The ease of fabrication is partly due to an easy demolding process which was achieved by a design choice that kept the molds flexible. The total thickness of the hydrogel samples, imposed by the PDMS spacer, was set to be larger than 100 µm to ensure that the cells would only sense the stiffness of the hydrogels [49]. We observed that polymerization was uninhibited if we used at least 1% of initiator (TEMED) and PDMS molds that were less than 50 µm thick [50].

The above-mentioned microstructures were successfully replicated in PA of 4 different stiffnesses, obtained by varying the acrylamide/bis-acrylamide concentrations (Table 1 and Fig. 3A). We calculated Young's moduli by fitting a Hertz model to the force-distance curves measured on the features (Fig. 3B). We obtained PA microstructures ranging from 3 ± 1 kPa to 145 ± 7 kPa (Figure 3C and Table 1), all of which faithful replicas of their mold geometries (Fig. 3D).

	% Acrylamide	% Bis-acrylamide	Young's modulus (kPa)
PA1	7.5	0.050	3 ± 1
PA2	7.5	0.075	13 ± 2
PA3	12	0.150	37 ± 6
PA4	12	0.600	145 ± 7

Table 1. Polyacrylamide hydrogel composition and resulting Young's modulus values measured by AFM. Mean ± SEM (N = 3)

This demonstrates that we have developed an original and simple method to reliably obtain PA hydrogels with topographical features of a biologically relevant size (<10 µm) and stiffnesses from within a biologically significant range (1-100 kPa).

3.2 Effect of swelling on microtopography size and shape.

Immediately after fabrication, the microstructures for all PA mixtures used in this study represented faithful reproductions of their corresponding mold geometries and dimensions. However, due to the natural meshwork architecture of hydrogels, they incorporate water until reaching an equilibrium, which leads to a swelling process that can change the shape and dimensions of the microtopographical structures fabricated on the hydrogel's surface. It is this swelling process that ultimately defines the feature morphology as has been shown previously for PEGDA [37] and PA [38]. To determine the swelling effects on the PA microstructures we monitored feature areas and shapes at 0, 24 and 48 h after fabrication. The topographical features changed both their size and shape over time (Figure 4A). We chose the posts and holes to evaluate the effects of swelling

because shape changes can be more easily quantified on these geometries. For all sizes and stiffnesses the holes shrank (by up to 50%) while the posts expanded (by up to 20%) during the first 24 hours. Between 24 h and 48 h we did not observe any more statistically significant changes (Figure 4B), which suggests that the equilibrium state had been reached after 24 h. In general, the softer the hydrogel the larger the change in area we observed for both holes and posts.

Interestingly, the smaller structures exhibited the larger relative change in area (Figure 4B). Whereas holes experienced larger area changes than posts, regardless of stiffness or size. These changes may amount to 50% for the softest and smallest holes.

The expansion or shrinkage of the microstructures due to swelling also produced noticeable changes in their shape (Figure 4A). While posts tended to lose their square shape and transformed into more convex and roundish features, the holes became more concave while swelling. These changes can be quantified using the S parameter (cf., Eq. (1)). In general, the shape changes in hole-like microstructures are more noticeable than in posts and softer structures exhibit larger deformations than stiffer ones. For all stiffnesses and sizes, posts transformed into more convex shapes ($S > 1$) whereas holes became more concave ($S < 1$). However, the 5 µm posts were already convex immediately after of fabrication and therefore did not significantly increase in convexity upon swelling (Fig. 4D).

3.3 Cell culture on PA hydrogels with controlled microtopography and stiffness.

Finally, we wanted to test whether our PA hydrogels could elicit cell responses to stiffness and microtopography that are similar to those previously reported. Screening for both topography and stiffness in a deconvoluted manner might reveal negative/positive feedbacks that are missed in conventional approaches that only screen one parameter (typically stiffness on flat substrates and topography on hard substrates). We chose to use lines for this test as linear topographies have been extensively used to test cell phenotype by measuring parameters such as cell alignment or elongation. This allowed for an easy comparison of our results to these previous findings.

3.3.1 Short-term fibroblast spreading, elongation and alignment.

We first employed a mouse embryonic-derived fibroblasts cell line (NIH 3T3) to test the validity of our approach and the potential impact on interrogating cell morphological changes in response to stiffness and microtopography over short time scales during cell spreading. We fabricated PA hydrogels containing topographical lines that were 5 µm wide and 1 µm high which are known to trigger cell alignment when tested on stiff substrates [23–25]. Since differences in stiffness had previously been reported to trigger differences in cell spreading area [51–53], we took advantage of the full potential of our system and fabricated line topographies of three different stiffnesses (13, 37, and 145 kPa). Before cell seeding, PA hydrogel surfaces were functionalized either with 20 µg/ml or 200 µg/ml of fibronectin solution, which did not altered stiffness in a significant manner (Supplementary Figure 1). NIH 3T3 fibroblasts were seeded on the functionalized PA hydrogels, and cell morphology was analyzed after 24 hours. We found that NIH 3T3 fibroblasts easily adhered and spread on the surfaces irrespective of hydrogel stiffness or topography (Figure 5A). Moreover, cell viability on PA hydrogels was 96%, similar that the one of glass (Supplementary Figure 2). By quantifying the morphological parameters, we could demonstrate that cells respond to both stiffness and topography. On the one hand, cell spreading area significantly increased with increasing substrate stiffness, both for the flat and patterned topographies independently of the amount of fibronectin (see supplementary table I for the statistical analysis). On the other hand, cells elongated (elongation index > 0.5) on the microstructured samples. Such elongation was stiffness dependent on substrates functionalized with 20 µg/ml of fibronectin and stiffness independent when fibronectin was incubated at 200 µg/ml concentration (see supplementary table I for the statistical analysis). Finally, cells aligned with the topographical lines (alignment index ~ 1) but did not show any statistically significant differences for the three stiffness values tested and the two fibronectin densities used (Figure 5B).

3.3.2 Long-term myotube formation and alignment.

To test the performance of our PA hydrogels presenting tunable physical cues at cellular processes that involve longer timescales, we made use of a mouse-derived myoblast cell line C2C12 which, under specific biochemical conditions, can differentiate into myotubes. It is known that either physiologically-like stiffness [54] or cell alignment produced by linear microstructures [55] can benefit the differentiation process of muscle tissue. We therefore produced post and line microstructures (5 µm wide and 1 µm high) on hydrogels with stiffnesses ranging from 3 to 37 kPa (values that had previously been reported to enhance myotube formation [54]). C2C12 cells were seeded ~~The~~ on hydrogels ~~were~~ functionalized with collagen type I, an extracellular matrix protein found in native muscle tissue and commonly used in C2C12 differentiation studies [54]. After 24 h, the C2C12 cells had adhered and spread on the topographical patterns for all three stiffnesses tested (Supplementary Figure 3 and Figure 5C). Interestingly, posts were visible even inside cells' cytoplasm, confirming their interaction with the topographical pattern. However, we observed that C2C12 cells on topographical posts were roughly aligned with the two orthogonal directions imposed by the posts, whereas cells on

lines elongated and aligned along the direction of the topographical pattern (Supplementary Figure 3). Therefore, differentiation studies were performed on linear microstructures. We left the cells to grow on the substrates for an additional 3 days before switching them to the differentiation medium. While cells reached confluency when cultured on the 13 and 37 kPa substrates, cells on the softest 3 kPa hydrogel grew less and did not reach confluency but aggregated into tightly packed regions (Figure 5C). Despite these differences in cell growth, the cells were visibly aligned with the topographical pattern on all three substrate types. After spending 1 week in the differentiation medium (i.e., after a total of 10 days of culture), myotube-like structures were becoming visible. They had aligned parallel to the topographical patterns on all substrates (Figure 5C). However, on the softest hydrogels myotubes were only present in those regions where C2C12 cells had reached confluency. To analyze myotube formation we evaluated the expression of the muscle differentiation marker myosin heavy chain (MHC) [54,55] by immunofluorescence after 10 days of culture (7 days after switching to differentiation medium). We found MHC positive cells in all conditions and cells were preferentially aligned on the topographically patterned areas (Figure 5D). We further tracked the differentiation process by monitoring the expression of the myogenic transcription factor MyoD and of Myosin Heavy Chain (MHC) [56] by immunofluorescence at different time points of the differentiation period on 13 kPa hydrogels (Supplementary Figure 4). We observed that the percentage of MyoD positive cells reached a maximum after 7 days of culture (4 days after switching to differentiation medium) and slightly decreased afterwards. On the contrary, MHC signal remained low (below 10% of surface coverage) until day 10 of culture (7 days after switching to differentiation medium), when it reached a surface coverage of 35%.

3.3.3 Primary intestinal epithelial cells on microstructured PA hydrogels.

To explore the ability of the microstructured PA hydrogels to sustain growth, migration, and differentiation of primary intestinal epithelial cells (IECs) we employed intestinal organoids-derived cells, including differentiated, proliferative, and adult intestinal stem cells. 5 µm line-patterned PA hydrogels of two different stiffnesses (13 kPa and 145 kPa) were functionalized with collagen type I and seeded with IECs. Although IECs are usually grown in 3D environments using Matrigel matrices, their growth into 2D epithelial monolayers has also been reported using plastic and glass supports coated with Matrigel or collagen type I thin layers [57,58]. Regardless of substrate stiffness, the IECs were able to attach and grow, forming an epithelial monolayer after 3 days of culture (Figure 6A).

Despite the softness of the basement membrane of the intestinal epithelium (~20 kPa) [59], our results suggest that IECs can be cultured on substrates possessing a wide range of stiffnesses. Immunofluorescence analysis for Ki-67 and cytokeratin20 showed the presence of both proliferative and differentiated cells in the monolayers formed on both substrate types (Supplementary Figure 5), demonstrating the preservation of the diverse cell population that is characteristic of intestinal epithelia. By monitoring the behavior of epithelial clusters for 5 hours using time-lapse microscopy, we found that cells on softer substrates (13 kPa) spread (or grew) less than the monolayers on harder hydrogels (145 kPa) (Figure 6B). While the clusters on 13 kPa lines expanded in area by 25% within 5 hours, clusters cultured on 145 kPa lines showed an area expansion that was twice as large (50%). Furthermore, actin accumulated along the topographical lines on both PA hydrogels (Figure 6A, yellow arrows). These results prompted us to analyze the potential effect of topography on cluster dynamics, by tracking the position of some epithelial colonies during 5 hours (Figure 6C). These clusters can move, change their shape, and eventually merge with other clusters. Some trajectories appeared to be biased in the direction of the lines.

Discussion

Microstructured PA hydrogels were generated by Capillary Force Lithography (CFL) using hybrid flexible PEN-PDMS molds (see Materials and Methods section and Fig. 1). In CFL, a thin film of thermoplastic polymer is put into contact with a mold, then the polymer is heated above its glass transition temperature which allows it to flow and fill the cavities of the mold by capillary force. Analogously, we poured the PA liquid solution into the purpose-built pools, thereby filling in the topographical structures of the mold by capillary force. After polymerization, the hydrogels were easily peeled off the PEN-PDMS mold thanks to its flexible nature. Using this approach we obtained PA hydrogels micropatterned with posts, holes and lines of 5 to 10 µm within a stiffness range from 3 to 145 kPa.

PA hydrogels are produced by binding acrylamide monomers with bis-acrylamide crosslinker in a redox radical polymerization process. This reaction is hindered by molecular oxygen which inhibits radical-induced polymerization because of its high reactivity with radicals [42]. The presence of an oxygen-permeable membrane such as PDMS generates a “deadzone” close to the oxygen source in which polymerization is inhibited [43]. This is why the microstructuring of PA hydrogels is typically performed using non-oxygen permeable silicon hard molds instead of PDMS [38–40]. These hard molds complicate the demolding process as peeling off a rigid mold might endanger the integrity of the topographical structures, especially when they are small and soft. To overcome these limitations, we employed flexible hybrid molds made of PDMS and PEN materials which

allowed for an easy detachment of the microstructured samples. In addition, PEN functions as an oxygen barrier thus preventing dead zones and the fact that it can be produced in thin layers allows the molds to maintain their flexibility. Our PEN-PDMS molds thus prevent external oxygen diffusion allowing polymerization to take place if there is enough local depletion of oxygen concentration to avoid radical scavenging. Actually, the use of either thicker PDMS molds (more oxygen) or lower TEMED concentrations (less radicals) that the ones used in the present work led to the inhibition of polymerization. Alternatively, PEN could be replaced by other materials that act as oxygen barriers. In the case that these materials are not flexible, such as glass, microstructures will be properly formed but can potentiatlly get damaged during the peeling off step.

These limitations that we bypassed with our methodology are typically addressed by using alternative materials such as PDMS. It has been used to replicate microstructured molds in an extremely simple and faithful manner since the 1990's [60] and its mechanical properties can be tuned to a certain extend by simply modifying the ratios of the pre-polymer and the cross-linker [34,50]. Previous studies have reported to replicate ~1 μm size structures on PDMS substrates ranging from 500 kPa to 2000 kPa [34], still far from the stiffness values that we report in here (3 kPa to 145 kPa). This range of compliances can be achieved by ultra-soft PDMS [61–65]. It can be as soft as 1 kPa [65], and it is suitable for mechanobiology experiments. These substrates are normally flat [62,65], but some efforts have been made to incorporate topographical patterns. However, those patterns are either large [64,66] or do not faithfully replicate the original mold when the topographical features are small (~1 μm) [61]. On the contrary, our method allows for the independent and precise control of both physical cues: topography and stiffness. Moreover, some soft PDMS formulations [67] behave as a viscoelastic material [68] and the mechanical properties at the cell-sensing range are different than at the macroscopic scale, leading to unexpected cellular responses [67,68]. In contrast, PA is an elastic hydrogel [52] with controlled stiffness and pore size that allows the study of stiffness-dependent cell behavior at the cellular mechanosensing range [68].

Since the level of cross-linking of the networks change depending on the ratio between acrylamide and bis-acrylamide and therefore pore size [68], it is expected to have different levels of liquid uptake into the hydrogel. We indeed observed that swelling decreased with stiffness, which agrees with the well-known fact that less crosslinked networks allow for greater PBS uptake and network expansion [38]. However, much less is known about the role of size and shape of the microstructures on swelling. We observed that swelling was dependent on the size of the topographical patterns. Small structures increased their area more than larger ones. This may be due to the higher surface to volume ratio in smaller structures which facilitates a higher water uptake and thus greater changes in area. When applying this technique to softer hydrogels and/or smaller topographical structures this may turn into a limiting factor. The shape of the structures was also important: changes in area of cavities were significantly larger than in convexities. This differential behavior for different geometries may be related to the fact that there is roughly 3 times more hydrogel around the holes than inside the posts. It should be taken into account when trying to replicate topographical microstructures of arbitrarily complex shapes. Overall, our results demonstrate that swelling significantly changes the dimensions and shapes of the microstructures produced in the PA hydrogels within 24 h of fabrication, by which time an equilibrium state is achieved. The extent of the morphological changes depends on feature geometry and size as well as on hydrogel stiffness. While posts and holes are particularly prone to deformation by swelling, mainly due to their confined 3D geometries and large surface to volume ratios, lines changed in width but did not exhibit any noticeable shape deformations (Supplementary Figure 6). The latter may be due to the use of relatively thick substrates which did not impose any restrictions on either lateral or vertical swelling. The line microstructures fabricated by our method thus preserved their geometries even for the softest materials (3 kPa, Supplementary Figure 6).

Overall, we obtained a porous material with controlled mechanical properties close to *in vivo* that can incorporate topographical features to impact cell behavior. When this topography is shaped as lines, the effect on cell behavior is known as contact guidance [23,24,30,31]. In this process, cells sense the topography and elongate, align and migrate along the direction parallel to the groves. Although the process is extensively reported, the exact mechanism by which this process takes place is still a subject of debate [69]. Moreover, most of the studies are performed on stiff materials, orders of magnitude larger than physiological values. By using our microstructured PA hydrogels we retrieved, in the short-term cellular response, the same effects attributed to individual changes in stiffness (cell area increasing with substrate stiffness [51,53,54]) and in topography (cell elongation and alignment [23,24,30,31]). In agreement with the observation that surface stiffness was independent of fibronectin density (Supplementary Figure 1), the dependence of cell spreading as a function of the stiffness was independent of the fibronectin density [52]. As well as cell alignment, which did not depend on cell stiffness nor fibronectin density. However, we observed that both physical cues had synergistic effects that did depend on the amount of fibronectin present on the surface. Topography mediated elongation was stiffness dependent at low fibronectin densities (Figure 5B), whereas such dependency was lost at higher fibronectin densities. This result suggests that both physical cues should be taken into

account when trying to decipher the topography sensing mechanism. In the long-term cellular response, our results suggest that effective cell differentiation, including myotube formation and alignment, are promoted by the synergistic effects of the microtopography and substrate stiffness. C2C12 cells cultured on PA microstructured hydrogels successfully formed myotubes that aligned parallel to the underlying topographical lines. Qualitatively, fluorescent signal of MHC immunostaining seems to be more expressed in stiffness values (~13kPa) that match the muscle tissue-like range as reported previously by Engler et al. [54]. We could also observe the time-dependent expression of differentiation markers. MyoD transcription factor expression increased along time, reaching a maximum 4 days after switching to differentiation medium. When MyoD signal started to slightly decrease, MHC increased to its maximum. Although these time-dependency follows the expected pattern during muscle differentiation [56], we did not observe myotube striation, which has been reported to appear in later differentiation stages (after 2 weeks of differentiation medium) [54]. Finally, we showed that our microstructured PA hydrogels could sustain growth of primary epithelial intestinal cells (IECs) from organoids derived from mouse intestine. To the best of our knowledge, our experiments represent the first time that IECs are grown onto thick substrates of PA hydrogels. Strikingly, spreading of IECs clusters was stiffness dependent. Similarly to what happened with NIH 3T3 fibroblasts, IECs grown on soft PA hydrogels spread less than when grown on stiff hydrogels. On the contrary, response to topographical lines was less dramatic. Actin accumulated on the topographical pattern, suggesting that the cytoskeleton of the epithelial cells was able to sense the presence of the topographical features regardless of the substrate stiffness. Also a bias in migration trajectories was observed. However, alignment was not as clear as the one observed for NIH 3T3 fibroblasts and C2C12 myoblasts, which have been reported to be more sensitive to topography compared to epithelial sheets [31]. Nevertheless, what we did clearly observed was the ability of PA microstructured hydrogels to stand the presence of both differentiated and proliferative cells, typical from IECs cultured on flat surfaces [70].

Conclusions

We have developed a reliable protocol to obtain topographical structures of different shapes (lines, square posts, and square holes) of biologically relevant sizes (5-10 μm) on polyacrylamide hydrogels of biologically significant stiffnesses (3-145 kPa). The different hydrogels were characterized in terms of stiffness, deformation of the topographical features over time due to swelling, and their performance as a culture platform for different cell types. We have seen that swelling significantly changed the dimensions of the microstructures in a stiffness-dependent manner within the first 24 hours, although the structures as such were preserved and their dimensions did not show any additional change after the initial 24 h of swelling. The impacts of swelling strongly depended on (i) the stiffness of the hydrogel (softer gels deformed more than stiffer ones), (ii) the type of topographical feature (holes deformed more than posts), and (iii) the size of the topographical pattern (while 5 μm structures showed a larger change in their area, 10 μm structures exhibited larger shape changes). Furthermore, we could demonstrate that these substrates were able to sustain the growth of different cell lines while influencing both their short- and long-term behavior. While all substrate types induced a contact guidance for the fibroblasts, the amount of cell spreading and elongation during the first 24 h was dependent upon substrate stiffness. At longer time scales, our micropatterned hydrogels allowed for the growth and differentiation of myoblasts while directing the formation of myotubes along the main orientations of the topographical patterns. Finally, we could demonstrate that primary mouse intestinal epithelial cells adhered and grew on the microstructured hydrogels while keeping both differentiated and proliferative cell populations active. Although the shape of the epithelia was not modified by the presence of the topographical patterns, the patterns were recognized by the actin cytoskeleton. In conclusion, we presented a bench-ready method to fabricate polyacrylamide hydrogels of biologically relevant stiffness with topographical features of biologically relevant sizes that can be applied to a range of cell-related studies that require an independent control of the stiffness and the geometry of the environment.

Acknowledgements

We thank Prof. Eduard Batlle from Institute for Research in Barcelona for providing the mouse intestinal samples. Funding for this project was provided by European Union's Horizon 2020 ERC grant agreement No 647863 (COMIET), the CERCA Programme/ Generalitat de Catalunya (2017-SGR-1079), and the Spanish Ministry of Economy and Competitiveness (TEC2017-83716-C2-1-R and the Severo Ochoa Program for Centers of Excellence in R&D 2016-2019). The collaboration of the MicroFabSpace from IBEC is gratefully acknowledged. The results presented here reflect only the views of the authors; the European Commission is not responsible for any use that may be made of the information it contains.

References

[1] Emonard H, Grimaud J A, Nusgens B, Lapiere C M and Foidart J M 1987 Reconstituted basement-membrane matrix modulates fibroblast activities in vitro. *J. Cell. Physiol.* **133** 95–102

[2] Gjorevski N, Sachs N, Manfrin A, Giger S, Bragina M E,

Ordóñez-Morán P, Clevers H and Lutolf M P 2016 Designer matrices for intestinal stem cell and organoid culture *Nature* **539** 560–4

[3] Petersen O W, Rønnov-Jessen L, Howlett A R and Bissell M J 1992 Interaction with basement membrane serves to rapidly distinguish growth and differentiation pattern of normal and malignant human breast epithelial cells. *Proc. Natl. Acad. Sci. U. S. A.* **89** 9064–8

[4] Chowdhury F, Li Y, Poh Y-C, Yokohama-Tamaki T, Wang N and Tanaka T S 2010 Soft Substrates Promote Homogeneous Self-Renewal of Embryonic Stem Cells via Downregulating Cell-Matrix Tractions *PLoS One* **5** e15655

[5] Nguyen T V, Sleiman M, Moriarty T, Herrick W G and Peyton S R 2014 Sorafenib resistance and JNK signaling in carcinoma during extracellular matrix stiffening. *Biomaterials* **35** 5749–59

[6] Engler A J, Sen S, Sweeney H L and Discher D E 2006 Matrix elasticity directs stem cell lineage specification. *Cell* **126** 677–89

[7] Lo C M, Wang H B, Dembo M and Wang Y L 2000 Cell movement is guided by the rigidity of the substrate. *Biophys. J.* **79** 144–52

[8] Sunyer R, Conte V, Escribano J, Elosegui-Artola A, Labernadie A, Valon L, Navajas D, García-Aznar J M, Muñoz J J, Roca-Cusachs P and Trepat X 2016 Collective cell durotaxis emerges from long-range intercellular force transmission *Science (80-.).* **353** 1157–61

[9] Munevar S, Wang Y L and Dembo M 2001 Traction force microscopy of migrating normal and H-ras transformed 3T3 fibroblasts *Biophys. J.* **80** 1744–57

[10] Trepat X, Wasserman M R, Angelini T E, Millet E, Weitz D A, Butler J P and Fredberg J J 2009 Physical forces during collective cell migration *Nat Phys* **5** 426–30

[11] Dembo M and Wang Y L 1999 Stresses at the cell-to-substrate interface during locomotion of fibroblasts *Biophys. J.* **76** 2307–16

[12] Uroz M, Wistorf S, Serra-Picamal X, Conte V, Sales-Pardo M, Roca-Cusachs P, Guimerà R and Trepat X 2018 Regulation of cell cycle progression by cell-cell and cell-matrix forces *Nat. Cell Biol.* **20** 646–54

[13] Nelson C M and Tien J 2006 Microstructured extracellular matrices in tissue engineering and development *Curr. Opin. Biotechnol.* **17** 518–23

[14] Dua H S, Shanmuganathan V A, Powell-Richards A O, Tighe P J and Joseph A 2005 Limbal epithelial crypts: A novel anatomical structure and a putative limbal stem cell niche *Br. J. Ophthalmol.* **89** 529–32

[15] Reya T and Clevers H 2005 Wnt signalling in stem cells and cancer. *Nature* **434** 843–50

[16] Solanas G and Benitah S A 2013 Regenerating the skin: A task for the heterogeneous stem cell pool and surrounding niche *Nat. Rev. Mol. Cell Biol.* **14** 737–48

[17] Provenzano P P, Eliceiri K W, Campbell J M, Inman D R, White J G and Keely P J 2006 Collagen reorganization at the tumor-stromal interface facilitates local invasion *BMC Med.* **4** 1–15

[18] Drifka C R, Loeffler A G, Mathewson K, Keikhosravi A, Eickhoff J C, Liu Y, Weber S M, John Kao W and Eliceiri K W 2016 Highly aligned stromal collagen is a negative prognostic factor following pancreatic ductal adenocarcinoma resection *Oncotarget* **7** 76197–213

[19] Dalby M J, Gadegaard N, Tare R, Andar A, Riehle M O, Herzyk P, Wilkinson C D W and Oreffo R O C 2007 The control of human mesenchymal cell differentiation using nanoscale symmetry and disorder *Nat. Mater.* **6** 997–1003

[20] Lee E A, Im S G and Hwang N S 2014 Efficient myogenic commitment of human mesenchymal stem cells on biomimetic materials replicating myoblast topography *Biotechnol. J.* **9** 1604–12

[21] Kubo K, Att W, Yamada M, Ohmi K, Tsukimura N, Suzuki T, Maeda H and Ogawa T 2008 Microtopography of titanium suppresses osteoblastic differentiation but enhances chondroblastic differentiation of rat femoral periosteum-derived cells *J. Biomed. Mater. Res. - Part A* **87** 380–91

[22] Rajnicek A and McCaig C 1997 Guidance of CNS growth cones by substratum grooves and ridges: effects of inhibitors of the cytoskeleton, calcium channels and signal transduction pathways. *J. Cell Sci.* **110** 2915–24

[23] Oakley C, Jaeger N A and Brunette D M 1997 Sensitivity of fibroblasts and their cytoskeletons to substratum topographies: topographic guidance and topographic compensation by micromachined grooves of different dimensions *Exp Cell Res* **234** 413–24

[24] Teixeira A I, Abrams G A, Bertics P J, Murphy C J and Nealey P F 2003 Epithelial contact guidance on well-defined micro- and nanostructured substrates. *J. Cell Sci.* **116** 1881–92

[25] Clark P, Connolly P, Curtis A S G, Dow J A T and Wilkinson C D W 1990 Topographical Control of Cell Behavior .2. Multiple Grooved Substrata *Development* **108** 635–44

[26] Park J, Kim D, Kim H, Wang C J, Kwak M K, Hur E, Suh K, An S S and Levchenko A 2016 Directed migration of cancer cells by the graded texture of the underlying matrix *Nat. Mater.* **15**

[27] Le-Berre M, Liu Y-J, Hu J, Maiuri P, Voituriez R, Chen Y and Piel M 2013 Geometric friction directs cell migration *Phys Rev Lett* **111** 198101

[28] Comelles J, Caballero D, Voituriez R, Hortigüela V, Wollrab V, Godeau A L, Samitier J, Martínez E and Riveline D 2014 Cells as active particles in asymmetric potentials: motility under external gradients *Biophys. J.* **107** 1513–22

[29] Caballero D, Comelles J, Piel M, Voituriez R and Riveline D 2015 Ratchetaxis: Long-Range Directed Cell Migration by Local Cues *Trends Cell Biol.* **25** 815–27

[30] Oakley C and Brunette D M 1993 The sequence of alignment of microtubules, focal contacts and actin filaments in fibroblasts spreading on smooth and grooved titanium substrata. *J. Cell Sci.* **106 (Pt 1** 343–54

[31] Ray A, Lee O, Win Z, Edwards R M, Alford P W, Kim D-H and Provenzano P P 2017 Anisotropic forces from spatially constrained focal adhesions mediate contact guidance directed cell migration *Nat. Commun.* **8** 14923

[32] Estévez M, Fernández-Ulibarri I, Martínez E, Egea G and Samitier J 2010 Changes in the internal organization of the cell by microstructured substrates *Soft Matter* **6** 582

[33] Mills C A, Fernandez J G, Martinez E, Funes M, Engel E, Errachid A, Planell J and Samitier J 2007 Directional Alignment of MG63 Cells on Polymer Surfaces Containing Point Microstructures *Small* **3** 871–9

[34] Tzvetkova-Chevolleau T, Stéphanou A, Fuard D, Ohayon J, Schiavone P and Tracqui P 2008 The motility of normal and cancer cells in response to the combined influence of the substrate rigidity and anisotropic microstructure. *Biomaterials* **29** 1541–51

[35] Mills C A, Escarré J, Engel E, Martinez E, Errachid A, Bertomeu J, Andreu J, Planell J A, Samitier J and Escarre J 2005 Micro-and nanostructuring of poly (ethylene-2, 6-naphthalate) surfaces, for biomedical applications, using polymer replication techniques *Nanotechnology* **16** 369

[36] Swift J, Ivanovska I L, Buxboim A, Harada T, Dingal P C D P, Pinter J, Pajerowski J D, Spinler K R, Shin J-W, Tewari M, Rehfeldt F, Speicher D W and Dennis E. Discher 2013 Nucler Lamin-A scales with tissue stiffness and enhances matrix-directed differentiation *Science (80-.).* **341** 1240104–15

[37] Garland S P, McKee C T, Chang Y R, Raghunathan V K, Russell P and Murphy C J 2014 A cell culture substrate with biologically relevant size-scale topography and compliance of the basement membrane *Langmuir* **30** 2101–8

[38] Charest J M, Califano J P, Carey S P and Reinhart-King C A 2012 Fabrication of substrates with defined mechanical properties and topographical features for the study of cell migration *Macromol. Biosci.* **12** 12–20

[39] Li Z, Gong Y, Sun S, Du Y, Lü D, Liu X and Long M 2013 Differential regulation of stiffness, topography, and dimension of substrates in rat mesenchymal stem cells *Biomaterials* **34** 7616–25

[40] Cheng X and Guo L J 2004 One-step lithography for various size patterns with a hybrid mask-mold *Microelectron. Eng.* **71** 288–93

[41] Nasrollahi S and Pathak A 2016 Topographic confinement of epithelial clusters induces epithelial-to-mesenchymal transition in compliant matrices *Sci. Rep.* **6** 18831

[42] Decker C and Jenkins A D 1985 Kinetic Approach of o2 Inhibition in Ultraviolet and Laser-Induced Polymerizations *Macromolecules* **18** 1241–4

[43] Tumbleston J R, Shirvanyants D, Ermoshkin N, Janusziewicz R, Johnson A R, Kelly D, Chen K, Pinschmidt R, Rolland J P, Ermoshkin A, Samulski E T and Desimone J M 2015 Continuous liquid interface of 3D objects *Science (80-.).* **347** 1349–52

[44] Plotnikov S V., Sabass B, Schwarz U S and Waterman C M 2014 *High-Resolution Traction Force Microscopy* vol 123 (Elsevier Inc.)

[45] Waterman-Storer C M 2001 Microtubule-organelle motility assays *Current Protocols in Cell Biology* ed B JS, D M, H JB, L-S J and K M Yamada (John Wiley & Sons, Ltd.)

[46] Fischer R S, Myers K A, Gardel M L and Waterman C M 2012 Stiffness-controlled three-dimensional extracellular matrices for high-resolution imaging of cell behavior *Nat. Protoc.* **7** 2056–66

[47] Alcaraz J, Buscemi L, Grabulosa M, Trepat X, Fabry B, Farré R and Navajas D 2003 Microrheology of human lung epithelial cells measured by atomic force microscopy. *Biophys. J.* **84** 2071–9

[48] Barker N, van Es J H, Kuipers J, Kujala P, van den Born M, Cozijnsen M, Haegebarth A, Korving J, Begthel H, Peters P J and Clevers H 2007 Identification of stem cells in small intestine and colon by marker gene Lgr5. *Nature* **449** 1003–7

[49] Kuo C H R, Xian J, Brenton J D, Franze K and Sivaniah E 2012 Complex stiffness gradient substrates for studying mechanotactic cell migration *Adv. Mater.* **24** 6059–64

[50] Mata A, Fleischman A J and Roy S 2005 Characterization of polydimethylsiloxane (PDMS) properties for biomedical micro/nanosystems *Biomed. Microdevices* **7** 281–93

[51] Pelham R J and Wang Y L 1998 Cell Locomotion and Focal Adhesions Are Regulated by the Mechanical Properties of the Substrate *Biol. Bull.* **194** 348–50

[52] Engler A, Sheehan M, Sweeney H L and Discher D E 2004 Substrate compliance vs ligand density in cell on gel responses *Biophys. J.* **86** 617–28

[53] Sunyer R, Jin A J, Nossal R and Sackett D L 2012 Fabrication of Hydrogels with Steep Stiffness Gradients for Studying Cell Mechanical Response *PLoS One* **7** 1–9

[54] Engler A J, Griffin M A, Sen S, Bönnemann C G, Sweeney H L and Discher D E 2004 Myotubes differentiate optimally on substrates with tissue-like stiffness: Pathological implications for soft or stiff microenvironments *J. Cell Biol.* **166** 877–87

[55] Choia Y S, Vincenta L G, Leea A R, Kretchmerc K C, Chirasatitsina S, Dobkeb M K and Engler A J 2012 The alignment and fusion assembly of adipose-derived stem cells on mechanically patterned matrices *Biomaterials* **33**

6943–51

[56] Chal J and Pourquié O 2017 Making muscle: Skeletal myogenesis in vivo and in vitro *Dev.* **144** 2104–22

[57] Wang Y, DiSalvo M, Gunasekara D B, Dutton J, Proctor A, Lebhar M S, Williamson I A, Speer J, Howard R L, Smiddy N M, Bultman S J, Sims C E, Magness S T and Allbritton N L 2017 Self-renewing Monolayer of Primary Colonic or Rectal Epithelial Cells *Cmgh* **4** 165-182.e7

[58] Thorne C A, Chen I W, Sanman L E, Cobb M H, Wu L F and Altschuler S J 2018 Enteroid Monolayers Reveal an Autonomous WNT and BMP Circuit Controlling Intestinal Epithelial Growth and Organization *Dev. Cell* **44** 624-633.e4

[59] Liao D, Yang J, Zhao J, Zeng Y, Vinter-Jensen L and Gregersen H 2003 The effect of epidermal growth factor on the incremental Young's moduli in the rat small intestine *Med. Eng. Phys.* **25** 413–8

[60] Mrksich M and Whitesides G M 1996 Using SAMS to Undestand the Interactions of Man-Made Surfaces with Proteins and Cells *Annu. Rev. Biophys. Biomol. Struct.* **25** 55–78

[61] Cesa C M, Kirchgeßner N, Mayer D, Schwarz U S, Hoffmann B and Merkel R 2007 Micropatterned silicone elastomer substrates for high resolution analysis of cellular force patterns *Rev. Sci. Instrum.* **78**

[62] Palchesko R N, Zhang L, Sun Y and Feinberg A W 2012 Development of Polydimethylsiloxane Substrates with Tunable Elastic Modulus to Study Cell Mechanobiology in Muscle and Nerve *PLoS One* **7**

[63] Style R W, Hyland C, Boltyanskiy R, Wettlaufer J S and Dufresne E R 2013 Surface tension and contact with soft elastic solids *Nat. Commun.* **4** 1–6

[64] Soiné J R D, Hersch N, Dreissen G, Hampe N, Hoffmann B, Merkel R and Schwarz U S 2016 Measuring cellular traction forces on non-planar substrates *Interface Focus* **6**

[65] Heinrichs V, Dieluweit S, Stellbrink J, Pyckhout-Hintzen W, Hersch N, Richter D and Merkel R 2018 Chemically defined, ultrasoft PDMS elastomers with selectable elasticity for mechanobiology *PLoS One* **13** 1–22

[66] Moraes C, Labuz J M, Shao Y, Fu J and Takayama S 2015 Supersoft lithography: Candy-based fabrication of soft silicone microstructures *Lab Chip* **15** 3760–5

[67] Trappmann B, Gautrot J E, Connelly J T, Strange D G T, Li Y, Oyen M L, Cohen Stuart M A, Boehm H, Li B, Vogel V, Spatz J P, Watt F M and Huck W T S 2012 Extracellular-matrix tethering regulates stem-cell fate *Nat. Mater.* **11** 642–9

[68] Wen J H, Vincent L G, Fuhrmann A, Choi Y S, Hribar K C, Taylor-Weiner H, Chen S and Engler A J 2014 Interplay of matrix stiffness and protein tethering in stem cell differentiation *Nat. Mater.* **advance on** 1–21

[69] Garcia-Arcos J M, Chabrier R, Deygas M, Nader G, Barbier L, Sáez P J, Mathur A, Vargas P and Piel M 2019 Reconstitution of cell migration at a glance *J. Cell Sci.* **132** jcs225565

[70] Altay G, Larrañaga E, Tosi S, Barriga F M, Batlle E, Fernández-Majada V and Martínez E 2019 Self-organized intestinal epithelial monolayers in crypt and villus-like domains show effective barrier function *Sci. Rep.* **9** 1–14

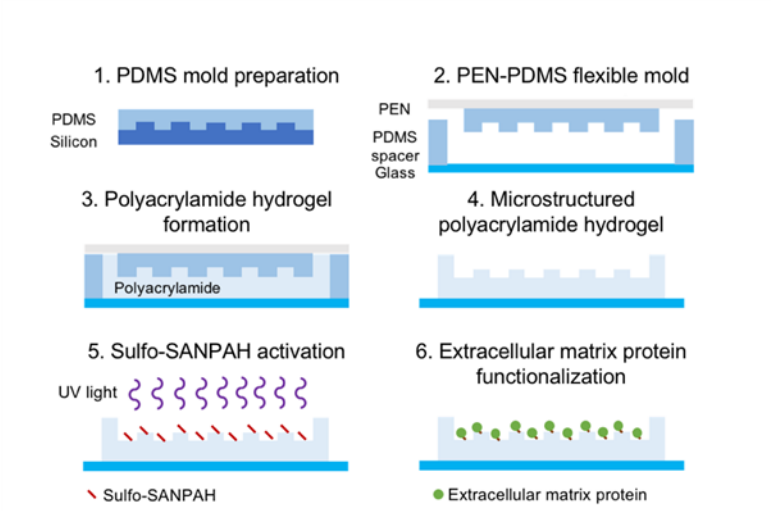

Figure 1. Schematic depicting the Capillary Force Lithography employed in this study. It uses flexible hybrid PEN-PDMS molds to obtain microstructured polyacrylamide hydrogels, which can then be functionalized for cell culture experiments.

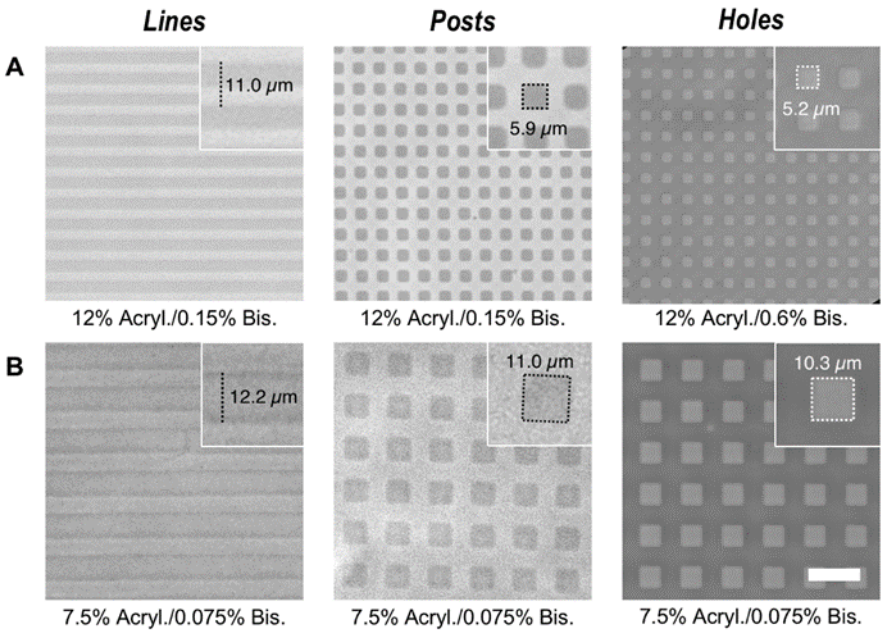

Figure 2. Phase contrast images of lines, posts, and holes in polyacrylamide hydrogels using different concentrations of Acrylamide/Bis-acrylamide polymers. (a) 5 μm-sized and (b) 10 μm-sized features. Scale bar 25 μm. Insets show actual sizes of the structures.

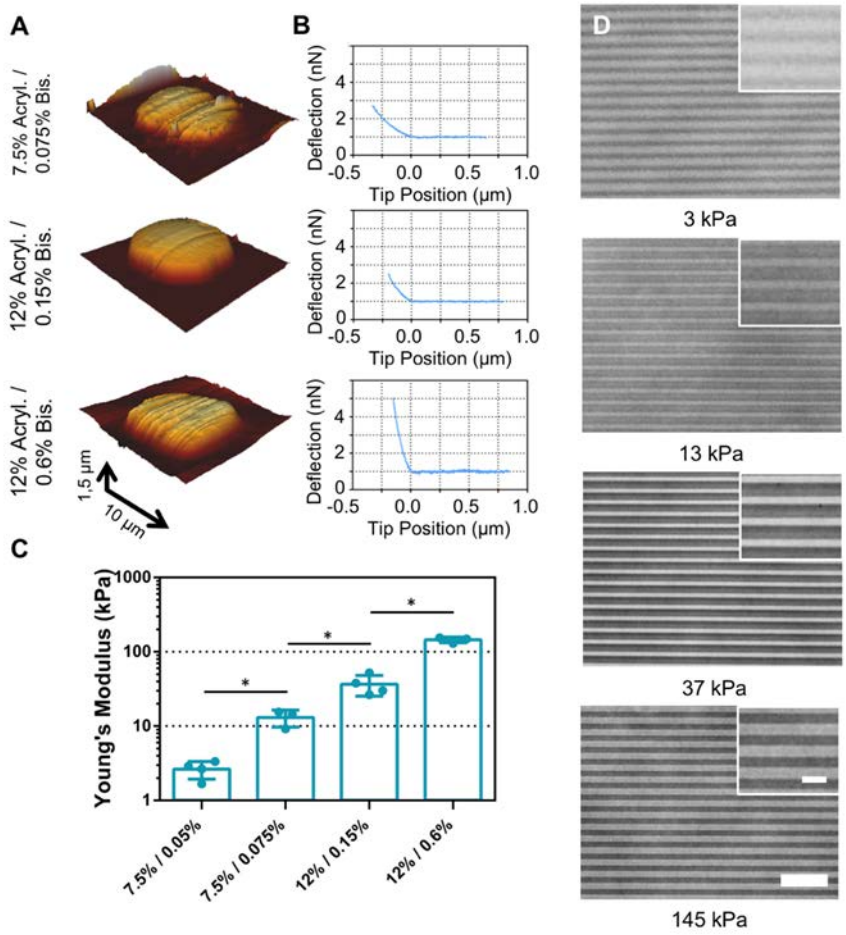

Figure 3. (A) 3-D reconstruction of the topographical features on the polyacrylamide surfaces. 10 µm posts of - from top to bottom - 7.5% Acrylamide/0.075% Bis-Acrylamide, 12% Acrylamide/0.15% Bis-Acrylamide, and 12% Acrylamide/0.6% Bis-Acrylamide. (B) Typical force-displacement curves of the AFM tip indenting the surface of the polyacrylamide hydrogels imaged in (A). (C) Young's moduli obtained from the AFM measurements for the different polyacrylamide compositions. Mean values ± SD. N = 3. (*) $p < 0.05$, Mann-Whitney test. (D) Phase contrast images of 5 µm wide lines of polyacrylamide hydrogels of different compositions. Scale bar: 40 µm. Insets show enlargements of the structures with a scale bar of 10 µm.

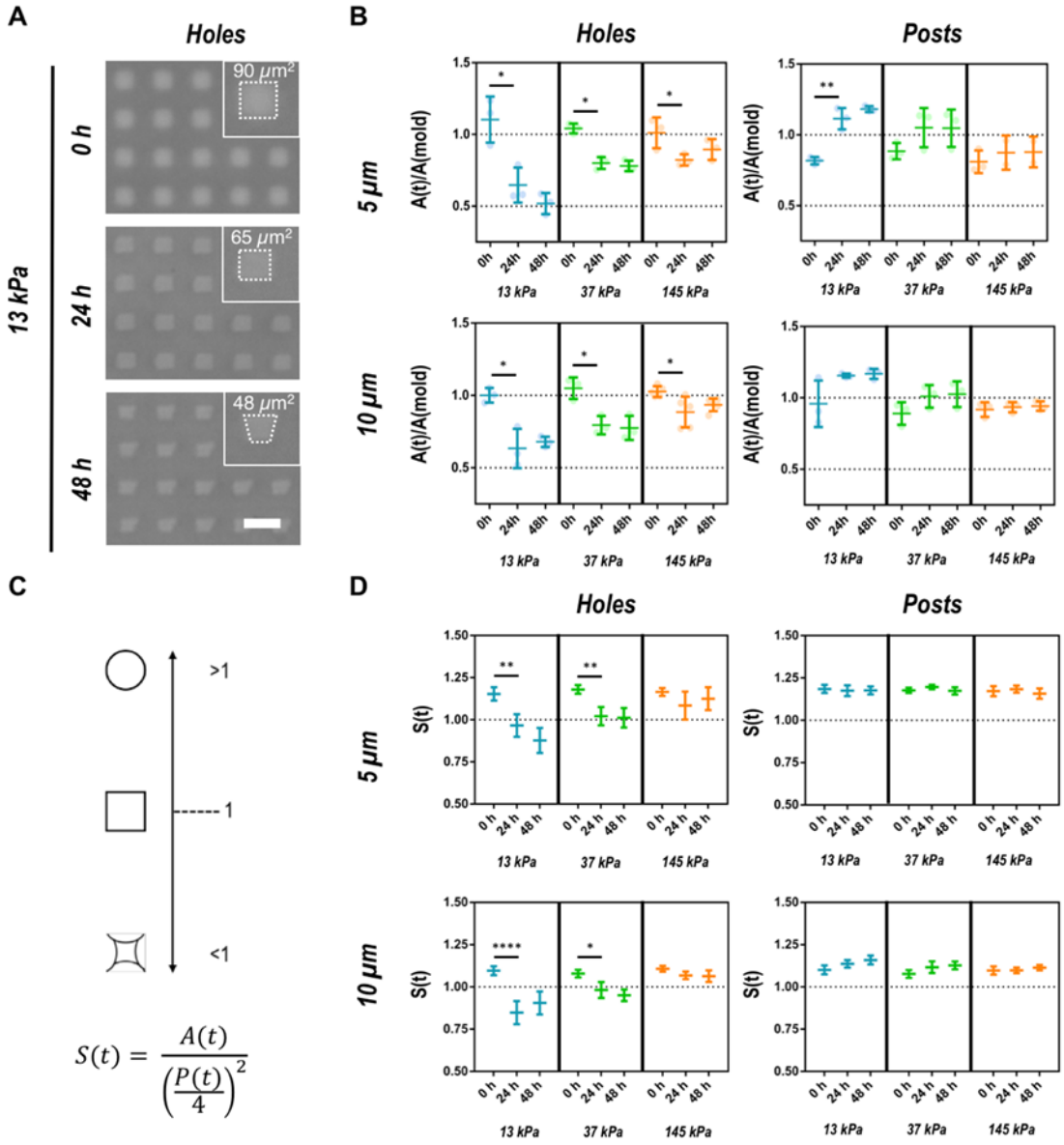

Figure 4. (A) Representative phase contrast images showing the temporal changes of 10 µm topographical patterns due to swelling. Insets show actual sizes of the structures. Scale bar: 20 µm. (B) Relative area changes of the topographical features over time due to swelling for three different stiffnesses. (*) $p < 0.05$ (**), $p < 0.01$, t-test. (C) Graphical representations of different values of the squareness parameter S (cf., Eq. (1)). (*) $p < 0.05$ (**), $p < 0.01$ (****) $p < 0.0001$, t-test. (D) Temporal evolution of the squareness parameter S. Data correspond to mean values ± SD. $N \geq 3$.

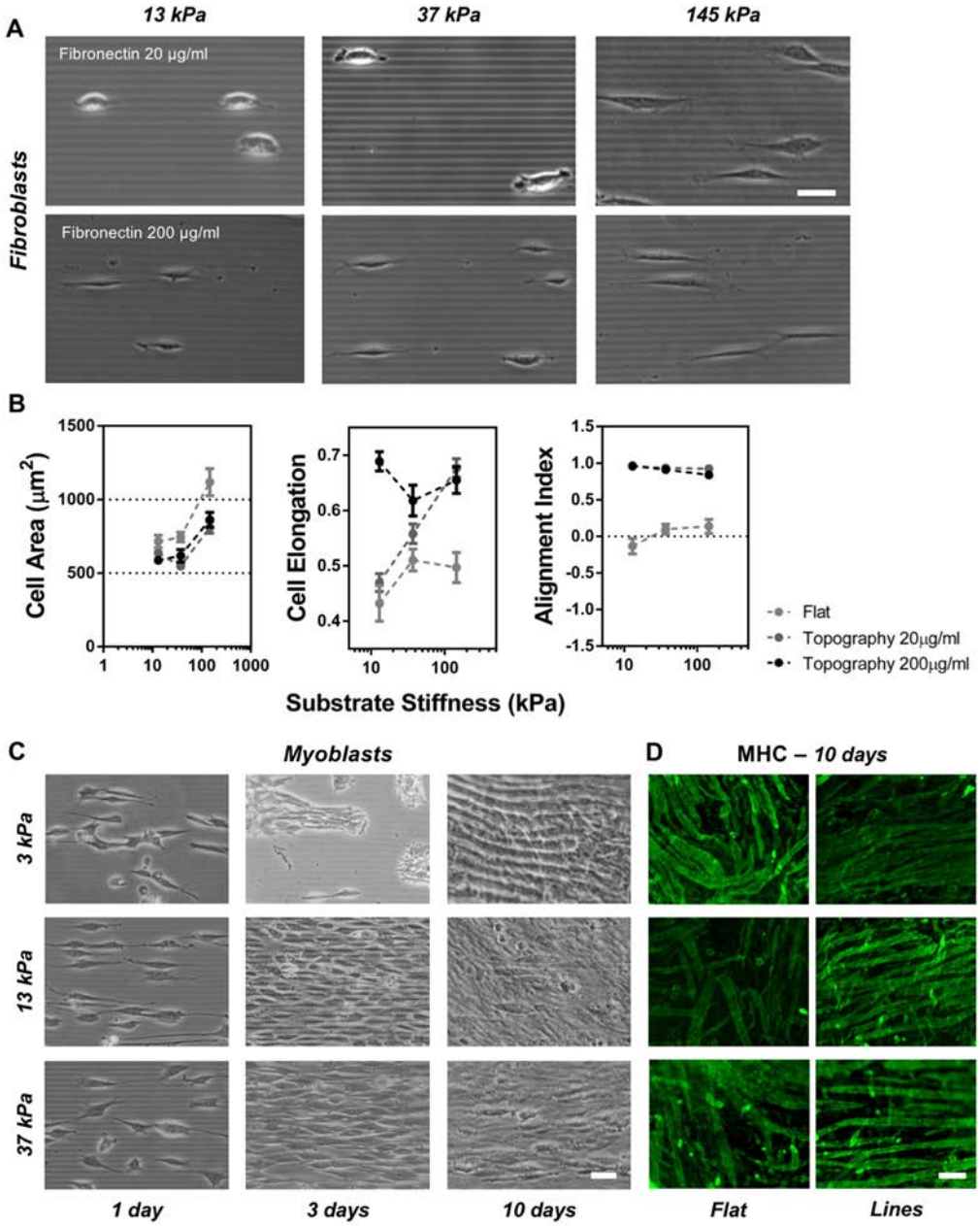

Figure 5. (A) Representative phase contrast images of NIH 3T3 fibroblasts on topographically modified polyacrylamide hydrogels functionalized with 20 µg/ml and 200 µg/ml of fibronectin, respectively. Scale bar: 45 µm. (B) Projected cell area, elongation, and alignment as a function of substrate stiffness. Mean value ± SEM. N = 3 experiments with n > 30 cells each. (C) Phase contrast images of C2C12 myoblasts on topographically modified polyacrylamide hydrogels. Scale bar: 40 µm. (D) Fluorescence images of myosin heavy chains on hydrogels of different stiffness. Scale bar: 50 µm.

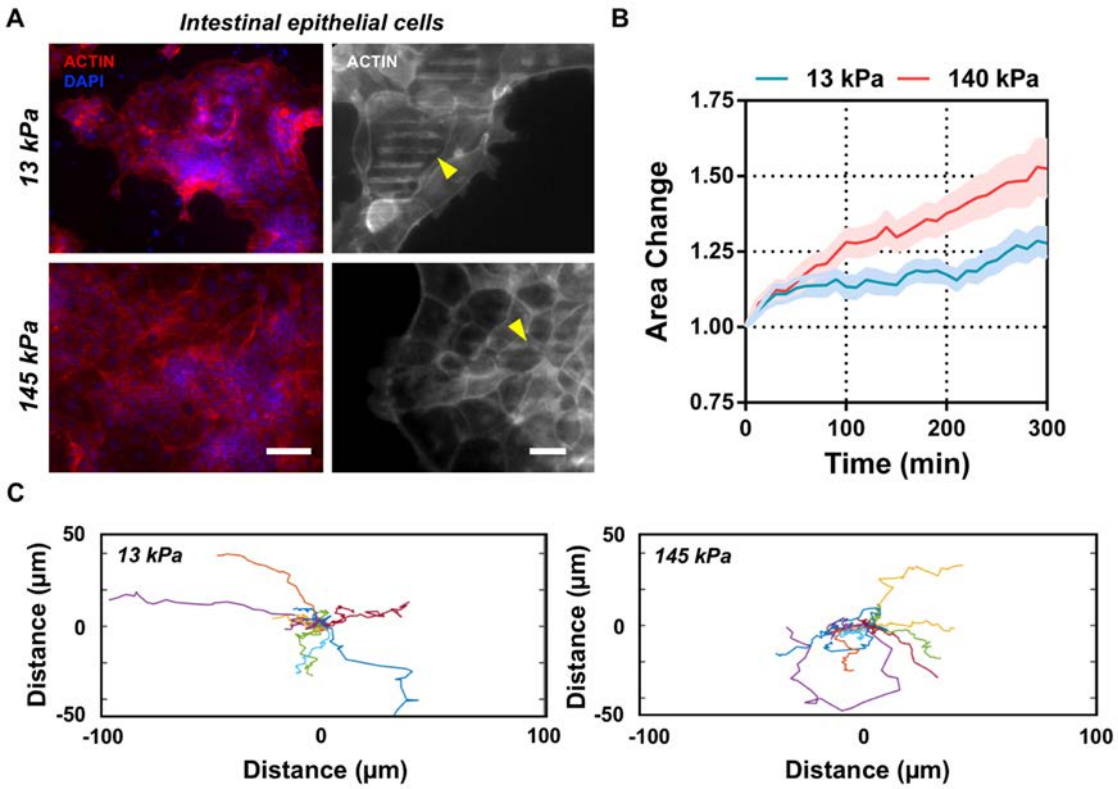

Figure 6. (A) Fluorescence images of mouse intestinal epithelial cells on microstructured (with 5 µm wide lines) PA hydrogels of two different stiffnesses: 13 kPa and 145 kPa. Actin is shown in red and nuclei in blue. Scale bar: 50 µm. (B) Change in area of the epithelial clusters over time, normalized to the initial area. Mean value ± SEM of N = 3 experiments. (C) Trajectories of epithelial clusters on topographical lines during 5 hours.